Electronic Supplementary Information

Lanthanide doping induced electrochemical enhancement of $Na_2Ti_3O_7$ anode for sodium-ion battery

Jiale Xia,[⊥a] Hongyang Zhao,[⊥ab] Weikong Pang,[⊥c] Zongyou Yin,[*d] Bo Zhou,[e] Gang He,[a] Zaiping Guo[c] and Yaping Du[*af]

[a.] Frontier Institute of Science and Technology, Xi'an Jiaotong University, 99 Yanxiang Road, Yanta District, Xi'an, Shaanxi, 710054, China. E-mail: ypdu@nankai.edu.cn

[b.] School of Science, Xi'an Jiaotong University, 28 Xianning West Road, Xi'an, Shaanxi, 710049, China.

[c.] Institute for Superconducting and Electronic Materials, University of Wollongong, 2522 NSW, Australia.

[d.] Research School of Chemistry, the Australian National University, Canberra, Australian Capital Territory 2601, Australia. E-mail: zongyou.yin@anu.edu.au

[e.] Department of Physics, Northwest University, Shaanxi, 710069, China.

[f.] School of Materials Science and Engineering & National Institute for Advanced Materials, Nankai University, 38 Tongyan Road, Haihe Education Park, Tianjin 300350, China.

⊥ These authors contribute equally.

Table of Contents

S1. Experimental details

Materials synthesis and characterization:

Micro-sized electrode material: The lanthanide doped $Na_2Ti_3O_7$ (NTO: 5‰Ln) electrode materials were synthesized by high-temperature solid-state method. 0.11 mol (4.4 g) of NaOH (99.9% purity) and 0.15 mol (11.98 g) of TiO_2 (99.99% purity), corresponding to a slight excess of NaOH with regard to the molar stoichiometry, together with 0.75 mmol $LaCl_3 \cdot 7H_2O$, $Ce(NO)_3 \cdot 6H_2O$, $Nd(NO)_3 \cdot 6H_2O$, $(CH_3COO)_3Sm \cdot 6H_2O$, $Gd(NO)_3 \cdot 6H_2O$, $(CH_3COO)_3Er \cdot 6H_2O$ and $(CH_3COO)_3Yb \cdot 6H_2O$ (99.99% purity, Beijing HWRK Chemical Company) respectively, were ball-milled at a speed of 600 rpm for 4 h. The obtained powder was then calcined in air at 900 °C for 12 h and cooled to room temperature in N_2 to obtain lanthanide doped $Na_2Ti_3O_7$. The pristine $Na_2Ti_3O_7$ was synthesized by similar process in the absence of lanthanide salt. All the starting materials were purchased and used without further purification.

Nano-sized $Na_2Ti_3O_7$: The $Na_2Ti_3O_7$ nanotubes were synthesized by hydrothermal method. Initially, 0.4g TiO_2 was dispersed in 40 mL 10 mol L^{-1} NaOH aqueous in a Teflon-lined stainless and stirred for 3 h. Then the autoclave was heated at 180°C for 24 h and then cooled to room temperature. The precipitate was collected with distilled water by a centrifuger. The above mixture was dried in an oven at 80 °C for 12 h.

Characterizations: The crystal structures of all the samples were characterized by X-ray diffraction (XRD) (Rigaku D/MAX-RB, Japan) using monochromatized Cu Kα radiation (λ=1.5418 Å). X-ray photoelectron spectra (XPS) were conducted using a PHI Quantera SXM instrument equipped with an Al X-ray excitation source (1486.6 eV). Thermogravimetric analysis (TGA) was performed in both air and N_2 using a Mettler Toledo TGA 1 simultaneous thermal analyzer. The morphologies were characterized by a field-emission scanning electron microscope (SEM) (FEI-F250, USA). High-resolution transmission electron microscopy (HRTEM) images were obtained using a transmission electron microscopy (Tecnai F20, USA).

Electrochemical measurements: The electrodes were prepared by mixing the active materials (60 wt.%), acetylene black (30 wt.%), polyvinylidene fluoride (PVDF) (10 wt.%) and an appropriate amount of N-methyl pyrrolidone (NMP) homogeneously and pasting onto the copper foil which acted as the current collector and then dried at 110 °C for 24 h under vacuum to remove the solvent. The coin-cells (CR 2032) were assembled with pure sodium foil as the counter electrode and a glass fiber as separator in an argon-filled glove box. The electrolyte adopted in the system is 1M $NaClO_4$ dissolved in a mixture of ethylene carbonate(EC)/ dimethyl ethylene carbonate (DMC) (1:1 Vol%) with 5% Fluoroethylene carbonate (FEC). The charge and discharge measurements were carried out on a Land BT2000 battery test system (Wuhan, China) in a voltage range of 0.01-2.5 V. Cyclic voltammetry (CV), electrochemical impedance spectra (EIS) and Mott-Schottky analysis were conducted on Metrohm Autolab PEGSTAT302N electrochemical workstation. The electronic conductivity characteristics were obtained using an Agilent B2902A Source Meter with a Micromanipulator 6150 probe station at room temperature.

S2. CV curves and charge/discharge profiles of NTO and NTO:Yb

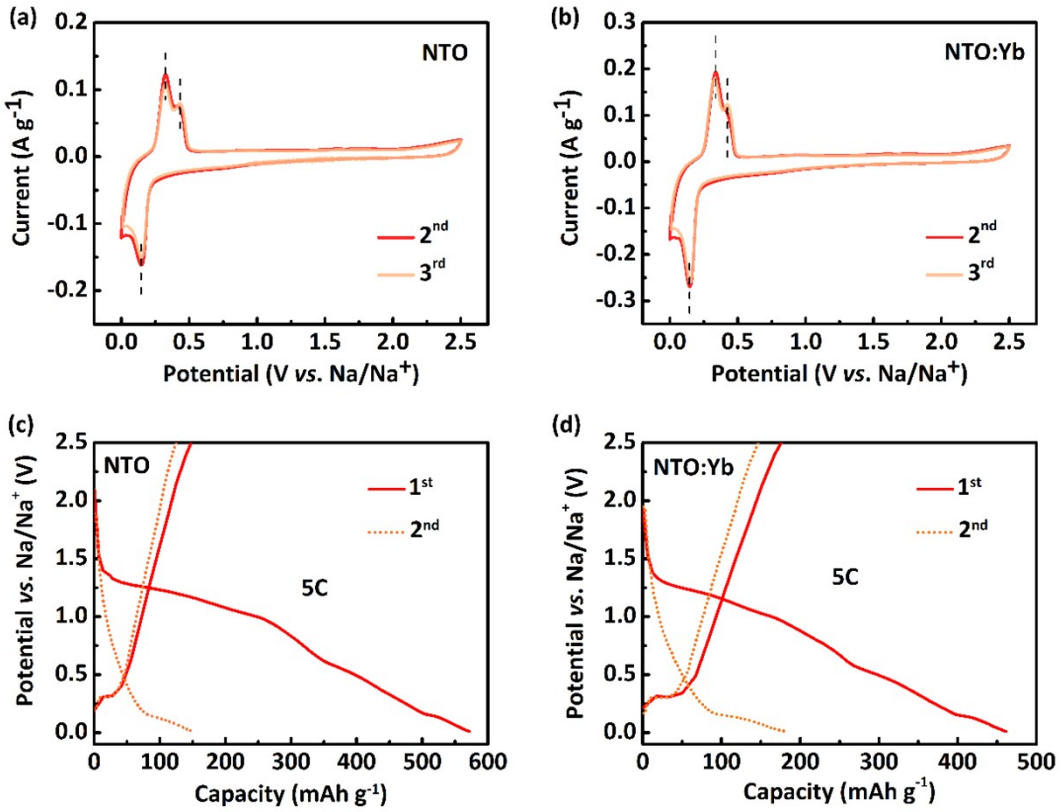

Figure S1. a) Cyclic voltammogram curves in a voltage range of 0.01-2.5 V for the NTO and b) NTO:Yb electrode at a scan rate of 0.1 mV s^{-1}. c) The 1st and 2nd charge/discharge curves of NTO and d) NTO:Yb electrode.

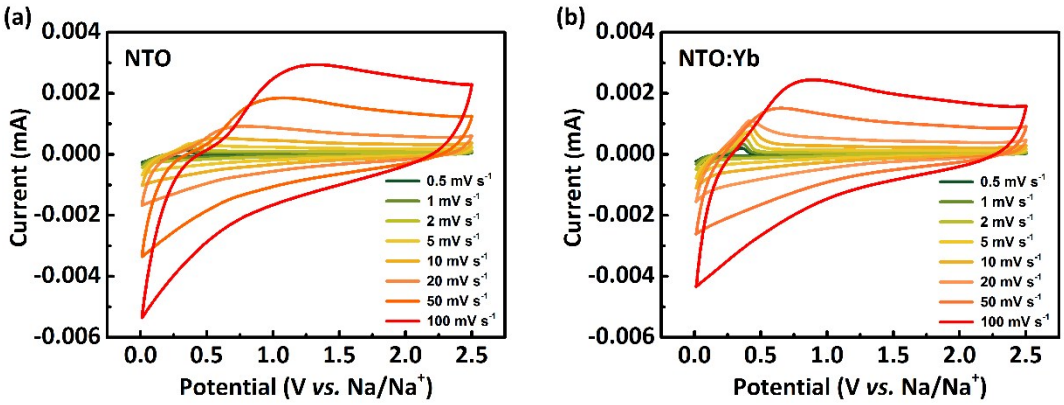

Figure S2. a) The Cyclic voltammogram from 0.5 to 100 mV s^{-1} for the NTO and b) NTO:Yb electrode.

S3. Electrochemical impedance spectra of NTO and NTO:Yb

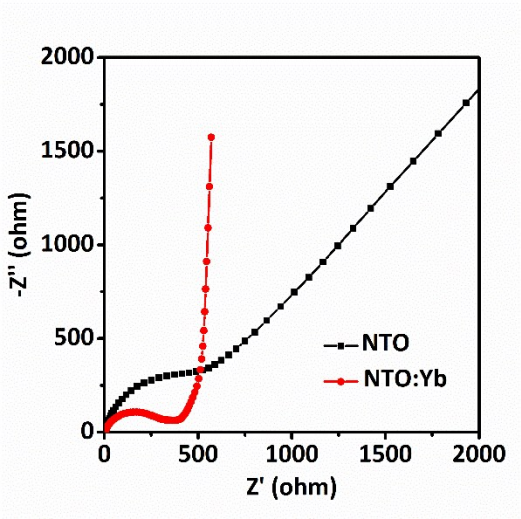

Figure S3. Electrochemical impedance spectra of NTO and NTO:Yb at room temperature.

S4. HRTEM and XRD refinement of NTO and NTO:Yb

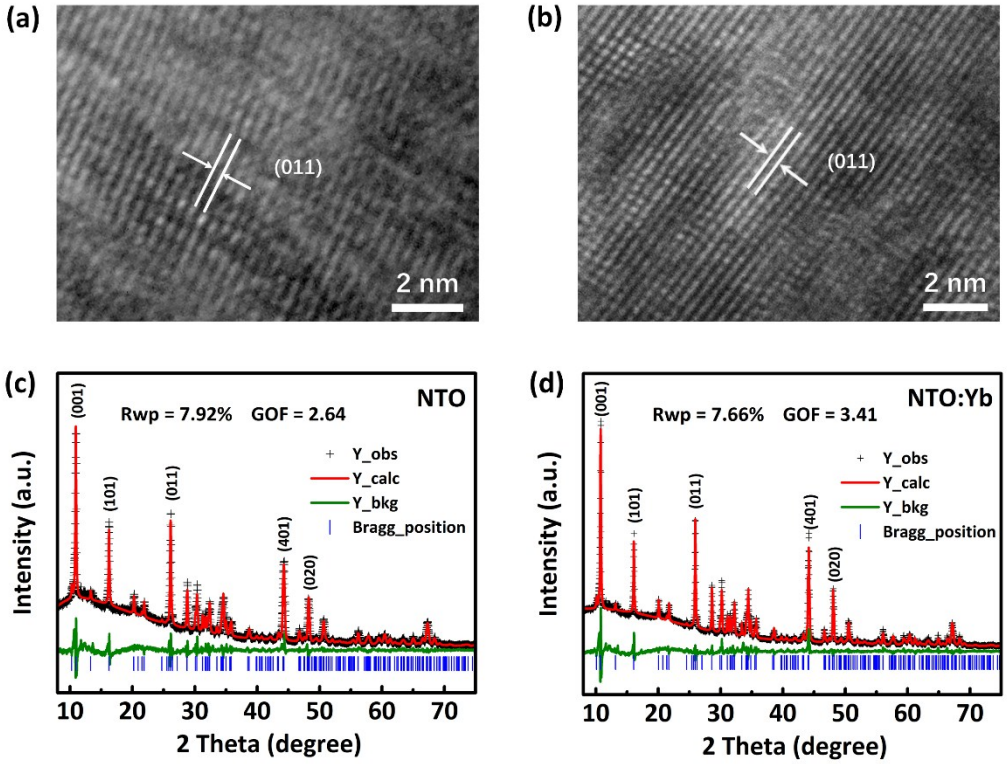

Figure S4. HRTEM image of a) NTO and b) NTO: Yb. The refinement XRD pattern of c) NTO and d) NTO: Yb. The refined cell parameters of NTO [a = 9.1332(7) Å, b = 3.8013(2) Å, c = 8.5763(7) Å, β = 101.58(1) °, Vol. = 291.69(4) Å^3] and NTO: Yb [a = 9.1217(5) Å, b = 3.7998(1) Å, c = 8.5599(5) Å, β = 101.59(1) °, Vol. = 290.65(4) Å^3] are obtained.

S5. TGA of NTO and NTO:Yb

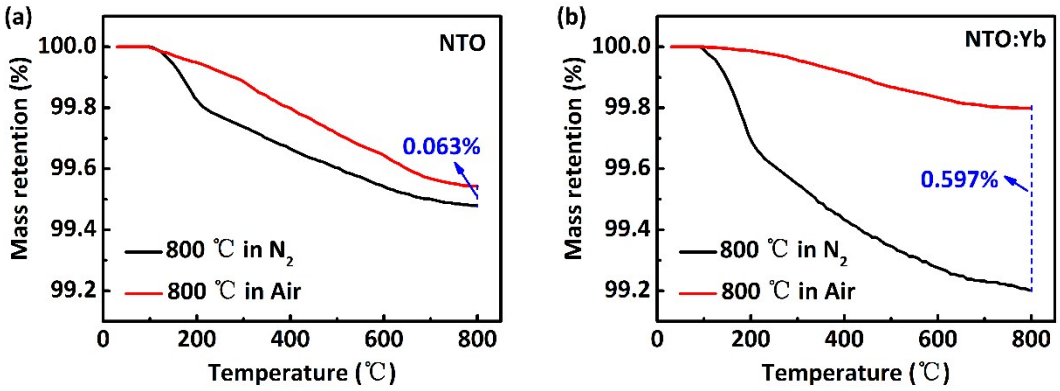

Figure S5. TGA analysis of a) NTO and b) NTO: Yb, respectively. (Flow of 100 mL/min and a ramping rate of 10 °C/min). The concentrations of oxygen vacancies were calculated from the difference in weight loss between the two TGA traces.

S6. Conductivites tested by four probes method

Table S1. The conductivities of NTO and NTO: Ln (Ln = La, Ce, Nd, Sm, Gd, Er, Yb)

	NTO	NTO:La	NTO:Ce	NTO:Nd	NTO:Sm	NTO:Gd	NTO:Er	NTO:Yb
Conductivity (10^{-7} S cm^{-1})	0.8065	1.5538	1.5536	0.9934	1.4085	1.6259	1.6287	1.7660

S7. Structure models for DFT calculations

The density functional theory (DFT) calculations were performed using the Vienna ab initio simulation package (VASP). With spin polarizations, the valence and core electron intercalations were described by the generalized gradient approximation (GGA) in the framework of the projector augmented-wave (PAW) method based on density functional theory (DFT). The gradient-corrected Perdew-Burke-Ernzeerhof (PBE) was employed for evaluating the electron exchange correlation energy.

Pristine $Na_2Ti_3O_7$: The electronic configurations Na $3s^1$, Ti $3p^6 3d^2 4s^1$, O $2s^2 2p^4$ were treated as the valence electrons. The energy cut-off for the plane-wave function and density were 500 eV. The irreducible Brillourin zone integration was performed using the 5×5×5 Monkhorst-Pack k-points grid with a Gaussian smearing of 0.1 eV near the Fermi level.
Yb doped $Na_2Ti_3O_7$: The electronic configurations Na $3s^1$, Ti $3p^6 3d^2 4s^1$, O $2s^2 2p^4$, Yb $4f^{14} 5s^2 5p^6 6s^2$ were treated as the valence electrons. The energy cut-off for the plane-wave function and density were 500 eV. A 1×1×3 supercell was adopted in the relaxations, and the 3×3×3 Monkhorst-Pack k-points grid was used for irreducible Brillourin zone integration with a Gaussian smearing of 0.1 eV near the Fermi level. The energy barriers of diffusion pathways were calculated by the nudged elastic band method with the energy and force convergence criterion 10^{-5} eV $Å^{-1}$ and 0.01 eV $Å^{-1}$, respectively.

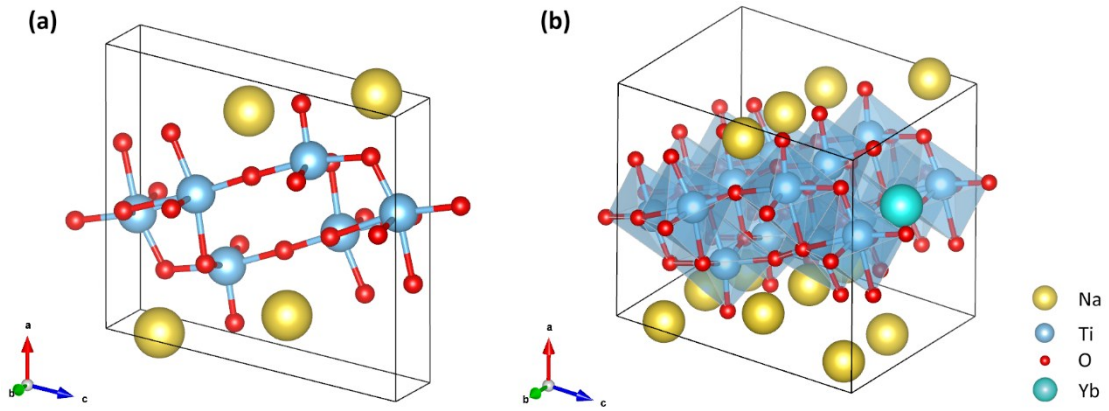

Figure S6. The structure models used in DFT calculations of a) NTO and b) NTO:Yb.

S8. Density of states (DOS) of NTO and NTO:Yb

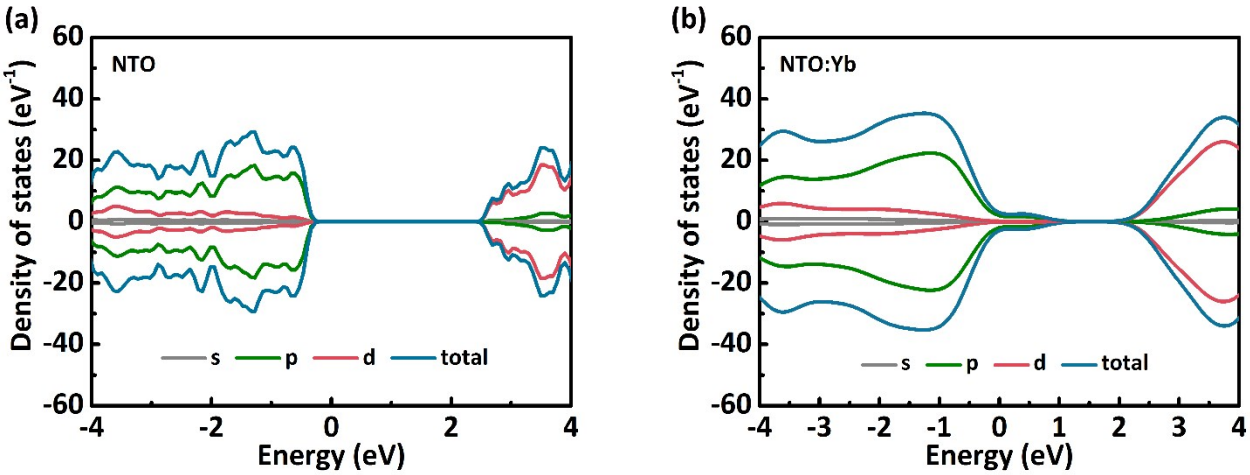

Figure S7. The density of states (DOS) for a) NTO and b) NTO:Yb.

S9. High-resolution XPS spectra of Ti 2p

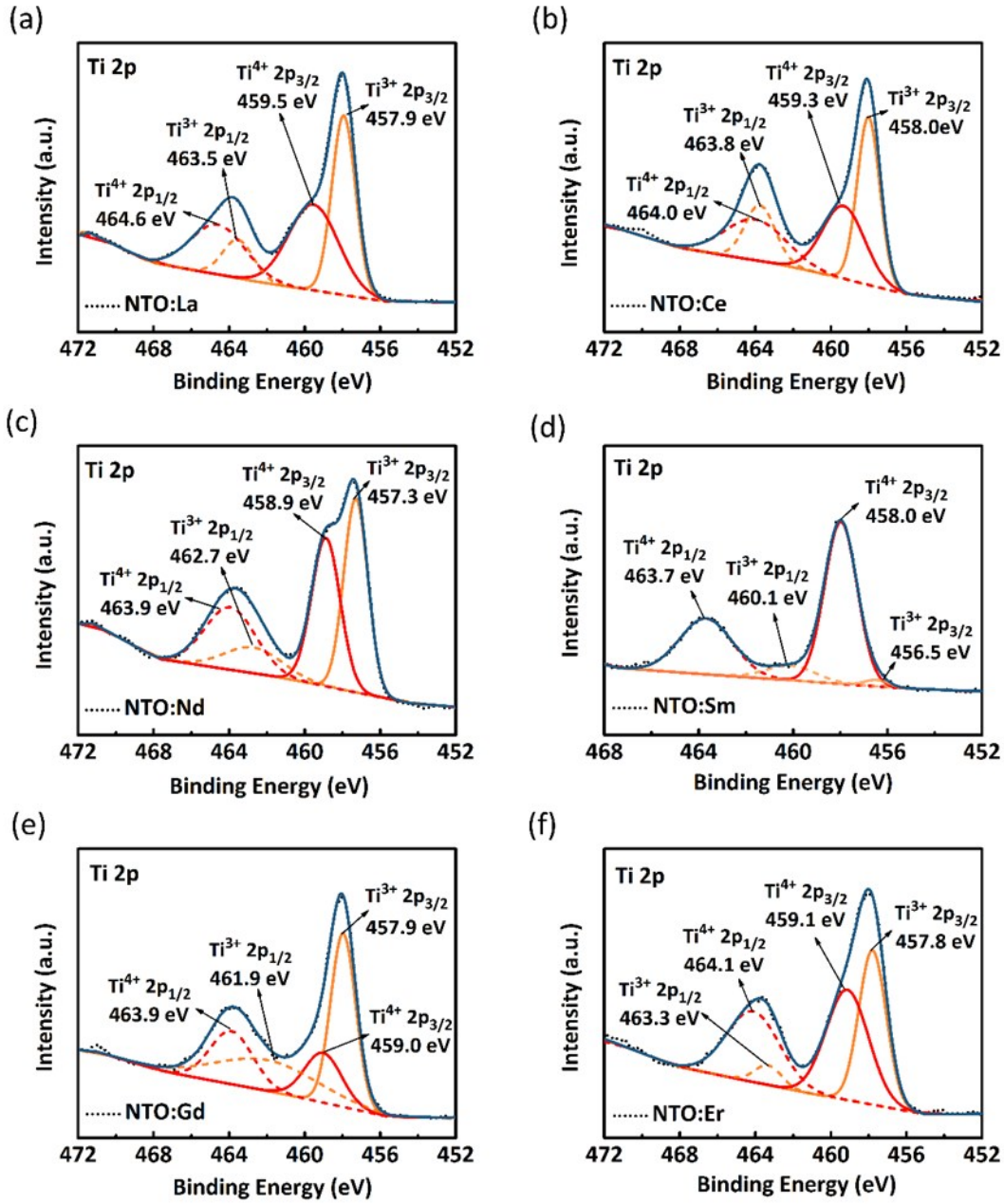

Figure S8. (a)~(f) Ti 2p XPS spectra of NTO:La, NTO:Ce, NTO:Nd, NTO:Sm, NTO:Gd and NTO:Er, respectively.

S10. High-resolution XPS spectra of Ln

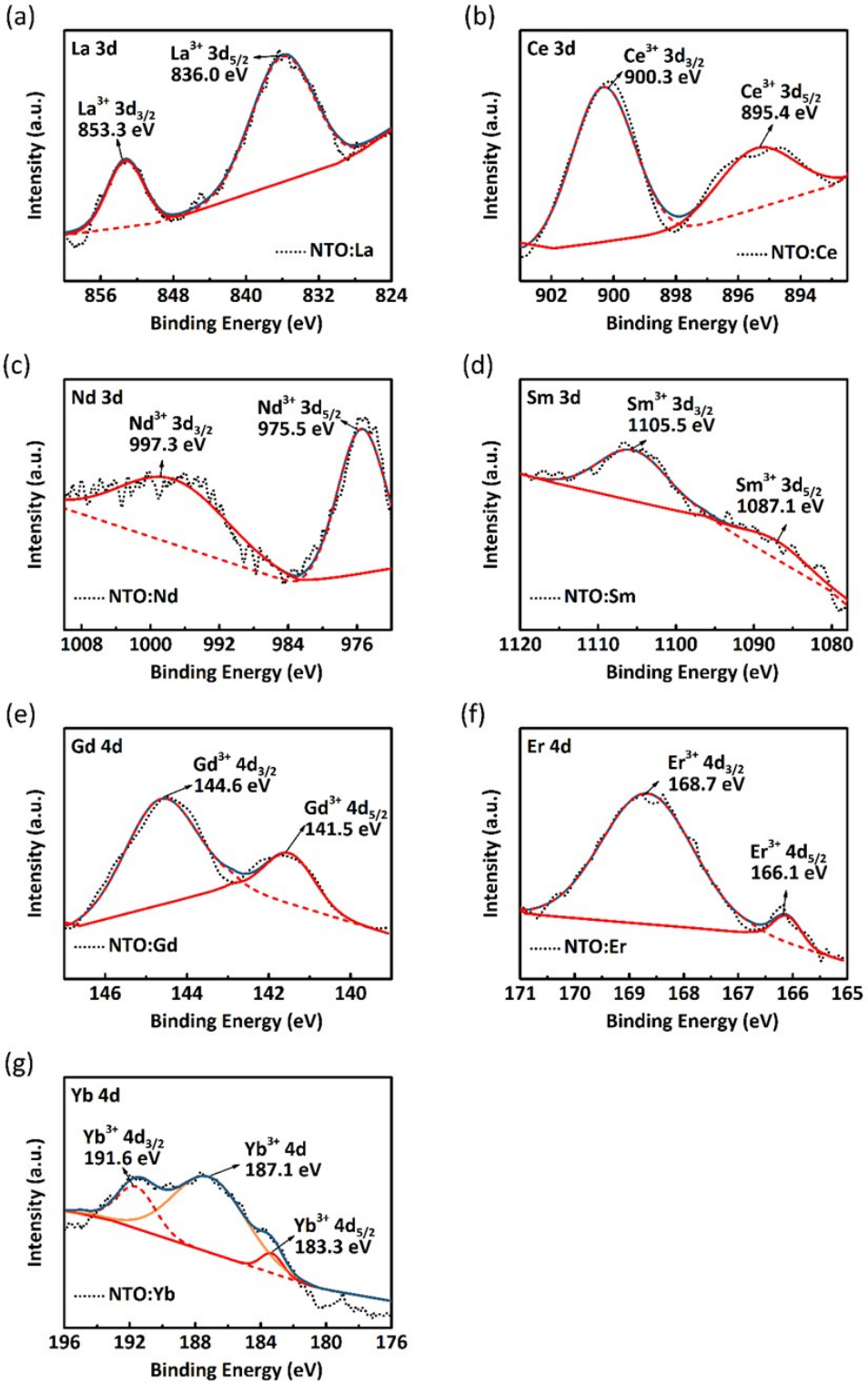

Figure S9. High-resolution XPS spectra of the La 3d, Ce 3d, Nd 3d, Sm 3d, Gd 4d and Er 4d, respectively.

S11. SEM images of NTO and NTO:Ln

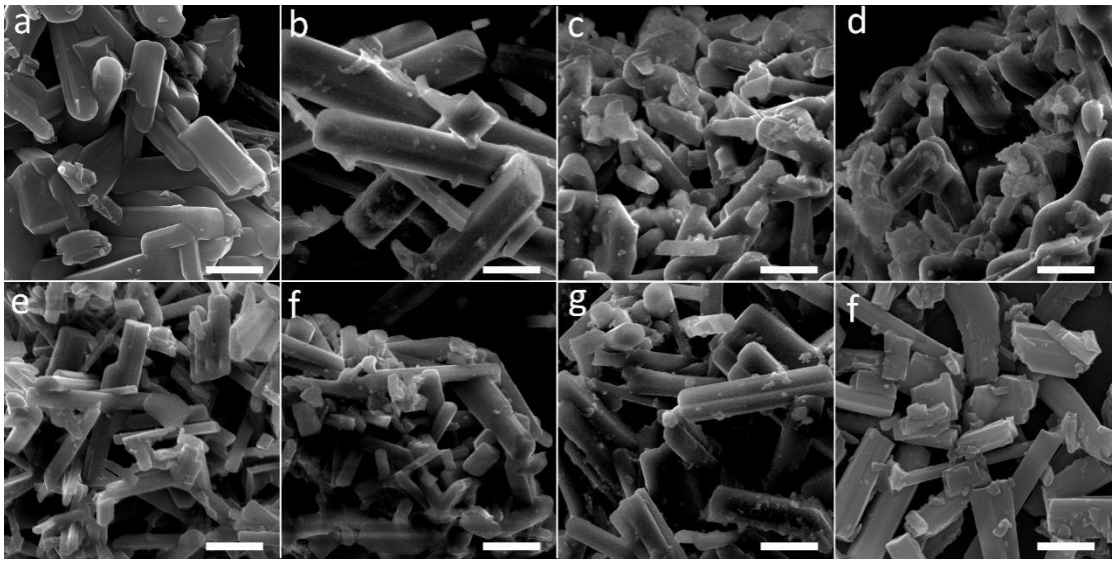

Figure S10. (a)-(f) SEM images of NTO, NTO:La, NTO:Ce, NTO:Nd, NTO:Sm, NTO:Gd, NTO:Er and NTO:Yb, respectively. The scale bar is 2 μm.

S12. Rate performance of NTO:Ln

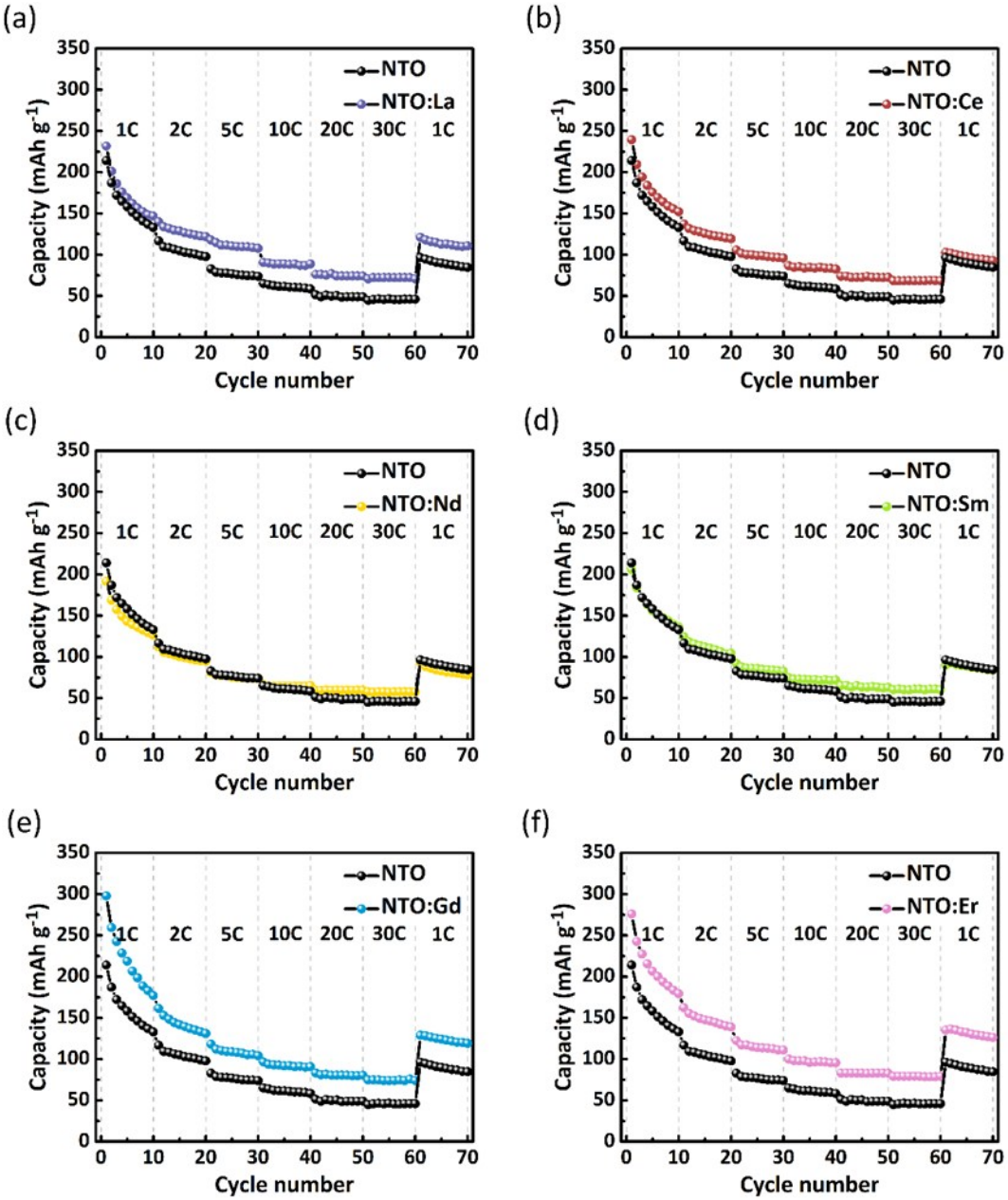

Figure S11. (a)~(f). The rate performance for NTO:La, NTO:Ce, NTO:Nd, NTO:Sm, NTO:Gd and NTO:Er electrode in a half cell, respectively.

S13. Cycle performance of NTO:Ln

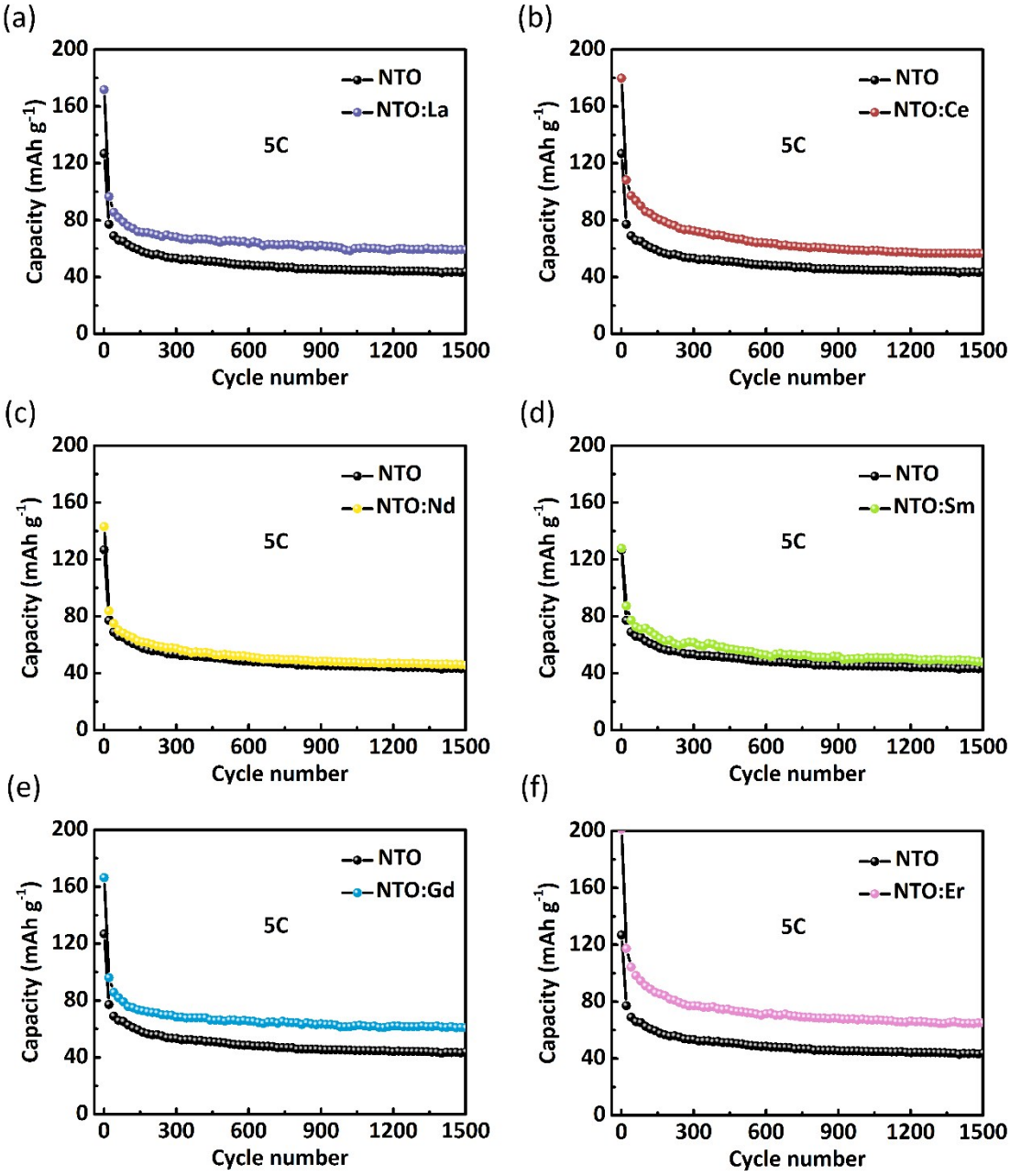

Figure S12. (a)~(f). The cyclic performance for NTO:La, NTO:Ce, NTO:Nd, NTO:Sm, NTO:Gd and NTO:Er electrode in a half cell, respectively.

S14. Mott-Schottky plots and calculated donor densities

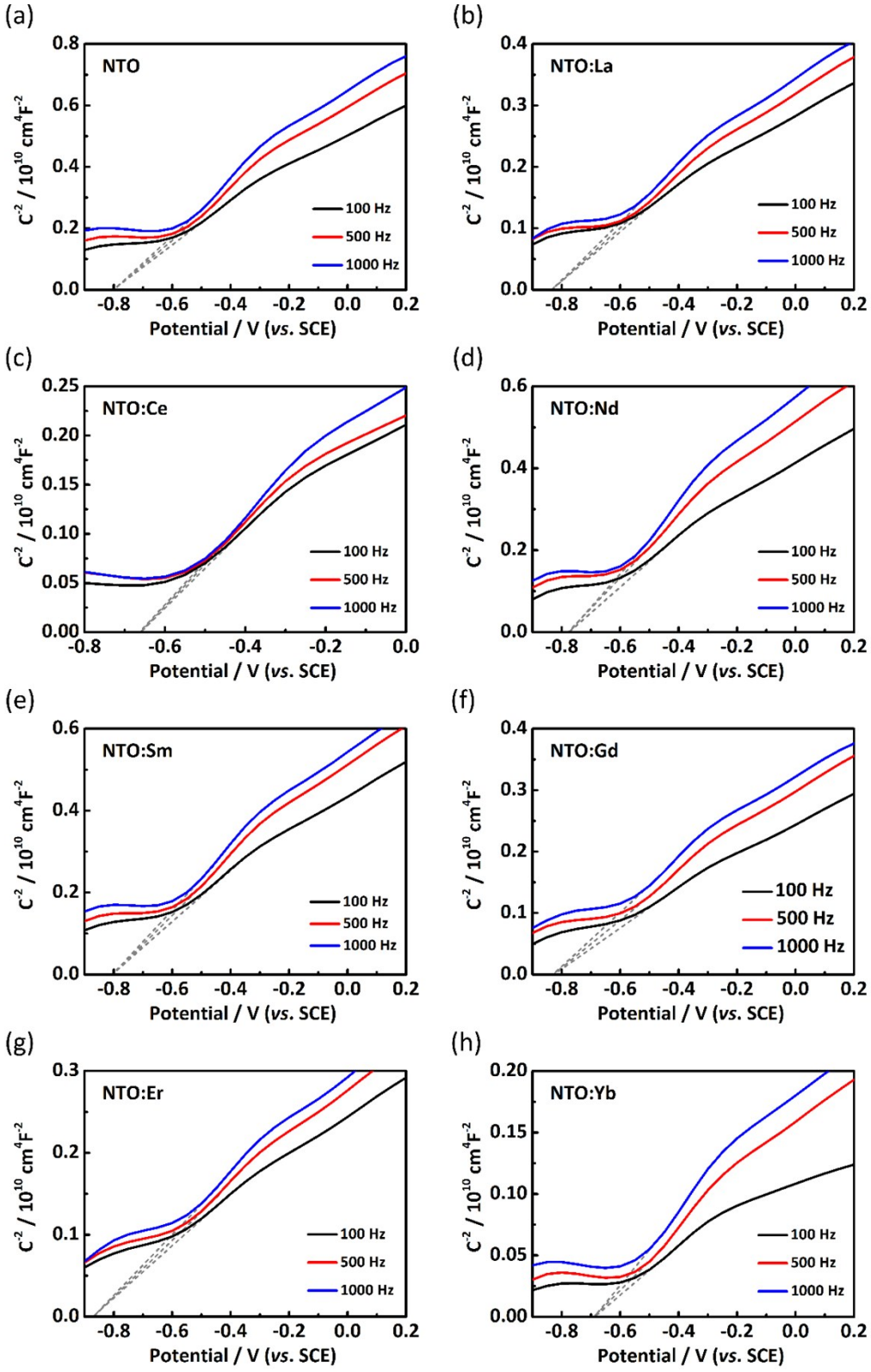

Figure S13. (a)-(h) Mott-Schottky plots of NTO, NTO:La, NTO:Ce, NTO:Nd, NTO:Sm, NTO:Gd, NTO:Er and NTO:Yb, respectively.

The equation for Mott-Schottky (M-S) analysis is:[1-3]

$$C^{-2} = 2 / (e\varepsilon\varepsilon_0 N_D) (E - E_{FB} - k_B T / q) \quad (1)$$

Where C is the capacitance of space charge layers, e is the electron charge (1.60×10^{-19} C), ε is the dielectric constant of the $Na_2Ti_3O_7$ (3.9), ε_0 is the vacuum permittivity (8.854×10^{-14} F/cm), N_D is the donor density (cm^{-3}), k_B is the Boltzmann constant (1.38×10^{-23} J K^{-1}). According to equation (1), the donor density N_D is inversely proportion to the slope (assume it as K) of M-S plots:

$$N_D = 2/e\varepsilon\varepsilon_0 K \quad (2)$$

Table S2. The donor densities of NTO and NTO: Ln (Ln = La, Ce, Nd, Sm, Gd, Er, Yb)

N_D (10^{26} cm^{-3})	100 Hz	500 Hz	1000 Hz
NTO	4.693528	3.52922	3.298429
NTO: La	9.434498	8.50212	8.145921
NTO: Ce	8.379593	8.03471	7.724411
NTO: Nd	5.592945	4.245827	3.951673
NTO: Sm	5.682179	4.391881	4.28842
NTO: Gd	9.839887	8.651704	8.483896
NTO: Er	11.52621	9.410184	8.634501
NTO: Yb	15.57816	11.1549	10.59103

S15. TGA of NTO:Ln

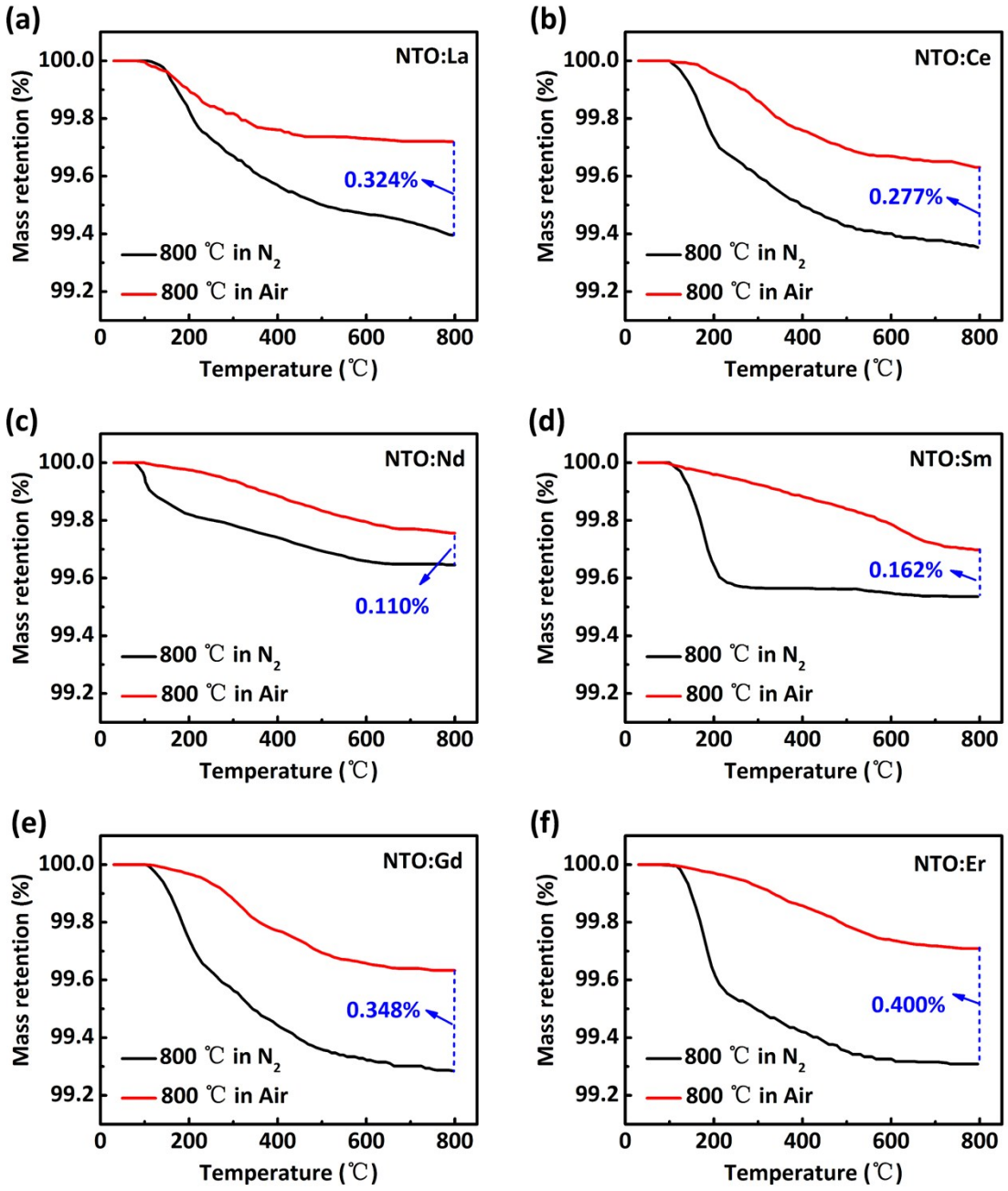

Figure S14. (a)-(f) TGA analysis of NTO:La, NTO:Ce, NTO:Nd, NTO:Sm, NTO:Gd and NTO:Er respectively. (Flow of 100 mL/min and a ramping rate of 10 °C/min). The concentrations of oxygen vacancies were calculated from the difference in weight loss between the two TGA traces.

References

1) Fattah-Alhosseini, A., Passivity of AISI 321 stainless steel in 0.5 M H2SO4 solution studied by Mott–Schottky analysis in conjunction with the point defect model. *Arabian J. Chem.* **2016,** 9, S1342-S1348.
2) Sazou, D.; Saltidou, K.; Pagitsas, M., Understanding the effect of bromides on the stability of titanium oxide films based on a point defect model. *Electrochimica Acta* **2012,** 76, 48-61.
3) Bott, A. W., Electrochemistry of semiconductors. *Current Separations* **1998,** 17, 87-92.